CO_2 Sorption

Deutsche Ausgabe: DOI: 10.1002/ange.201607076
Internationale Ausgabe: DOI: 10.1002/anie.201607076

Giant Hysteretic Sorption of CO_2: In Situ Crystallographic Visualization of Guest Binding within a Breathing Framework at 298 K

*Prem Lama, Himanshu Aggarwal, Charl X. Bezuidenhout, and Leonard J. Barbour**

Abstract: *A dynamic Zn^{II}-MOF has been shown to exhibit extreme breathing behavior under gas pressure. The very narrow pore form of the activated framework opens up in the presence of carbon dioxide, thus making it a suitable material for CO_2 capture. Sorption of CO_2 at 298 K and relatively high pressure clearly shows a two-step isotherm with giant hysteresis for the second step. In-situ single-crystal diffraction analysis was carried out under CO_2 gas pressure at 298 K using an environmental gas cell in order to visualize the interaction between CO_2 and the host framework. The results are well supported by pressure-gradient differential scanning calorimetry (P-DSC) and variable-pressure powder X-ray analysis. Theoretical calculations have been carried out in order to further back up the crystallographic data.*

Carbon dioxide is one of the major green-house gases and its increasing concentration in the atmosphere is raising concerns about global warming.[1] Since most of our energy demands are still being met by burning fossil fuels, there is growing interest in developing new reusable materials that can selectively capture CO_2, thus reducing its emissions into the atmosphere. Metal–organic frameworks (MOFs),[2] among various other porous materials,[3] are considered promising candidates for gas sorption[4] and separation of substances.[5] Owing to their large surface areas[6] and tunable pore sizes,[7] MOFs have been successfully employed for the sorption of a variety of gases, especially carbon dioxide.[8]

One of the main advantages of MOFs over conventional porous materials, such as zeolites[9] and activated carbons,[10] is their flexibility.[11] Flexible MOFs not only display unique dynamic behavior[12] (shrinking and expansion), but they also show selective sorption[13] properties that make them potentially suitable for sensing[14] and separation of gases.[5,13] The selectivity of a MOF towards a particular gas can be due to either the size/shape exclusion effect[15] or the change in pore size/shape upon adsorption.[12a,16] Sorption studies involving flexible/dynamic MOFs are particularly interesting with regard to hysteretic[17] and breathing[12] (gate-opening) behavior. The gate-opening phenomenon is generally assumed to be indicative of structural transformations during the adsorption process. The structural changes associated with gate-opening under gas loading conditions are challenging to characterize, yet important in terms of understanding host–guest interplay (i.e. as compared to rigid frameworks that typically show type I isotherms).[13b]

Researchers typically use various techniques such as IR spectroscopy,[17a,18] NMR,[19] and powder X-ray diffraction[20] in order to identify the interactions between gases and host framework materials. Although all of these techniques have been used extensively to ascertain the presence of gas molecules inside the MOF structures, the use of in situ single-crystal X-ray diffraction (SCXRD) is superior because it can often provide unequivocal structural information relating to host–guest interactions.[21] However, SCXRD presents a technical challenge[12d] as it involves exposing a single crystal to a particular gas pressure within a confined environment during the diffraction experiment, with the added requirement of maintaining crystal singularity. However, if the gas loaded structure can be elucidated at a particular pressure using SCXRD analysis, the host–guest interactions can be evaluated. In the case of MOFs with open metal sites, adsorption and selectivity for CO_2 gas is usually due to favorable interactions with the metal centers.[22] However, when no such open metal sites are present, uptake will depend on dispersion and electrostatic interactions between the host framework and the guest molecules. Here we present direct evidence of CO_2 molecules interacting with a breathing MOF as determined by means of in situ SCXRD analysis using an environmental gas cell.[21b] The Zn^{II}-framework, $\{Zn(tp)(1,2,3\text{-tz})\cdot x\,DMF\}_n$ (**1**) (tp = terephthalate and 1,2,3-tz = 1,2,3-triazolate), shows structural flexibility upon desolvation with retention of crystal singularity and is therefore ideal for the study of breathing behavior under high gas pressures.[11c,23]

The asymmetric unit of the desolvated complex (**1a**) comprises one tp, one 1,2,3-tz and two crystallographically independent Zn^{II} ions (one with half occupancy and the other with full occupancy). One zinc center (Zn1) is octahedrally coordinated to four oxygen atoms from four different tp ligands and two nitrogen atoms from two different 1,2,3-tz units. The second Zn center (Zn2) is tetrahedrally coordinated to two oxygen and two nitrogen atoms from two different carboxylate and 1,2,3-tz ligands (Figure S1 in the Supporting Information). In **1a** the overall dimensions of the pores, formed by the Zn clusters and the tp units within the 4,4-Zn-tp network, are entirely different from those of the as-synthesized complex **1**[11c]. The Zn-tp-Zn connectivity of the 4,4-Zn-tp network resembles a rhombus (Figure S2). The short diagonal of this rhombus shrinks from 11.51(1) Å (**1**) to 7.95(1) Å (**1a**),[11c] whereas the long diagonal expands slightly from 19.09(1) Å (**1**) to 19.76(1) Å (**1a**). This trellis-like

[*] Dr. P. Lama, Dr. H. Aggarwal, C. X. Bezuidenhout, Prof. L. J. Barbour
Department of Chemistry and Polymer Science
University of Stellenbosch
Matieland 7602 (South Africa)
E-mail: ljb@sun.ac.za

Supporting information for this article can be found under: http://dx.doi.org/10.1002/anie.201607076.

mechanism[12c] results in an overall reduction of the solvent accessible volume (Table S1).

The low pressure CO_2 and N_2 sorption measurements for **1a** have previously been reported in the literature.[11c,23] However, to date there have been no reports on high pressure sorption studies for this known framework. To this end we carried out sorption analysis with CO_2 and N_2 at 298 K up to a pressure of 50 bar. The sorption isotherm for N_2 shows very little uptake up to 50 bar, and no hysteretic or gate-opening step is apparent. However, in the case of CO_2, the sorption isotherm consists of two major steps. The first step occurs with an onset pressure of 0.8 bar, with CO_2 uptake leveling out between 20–35 bar; at 35 bar CO_2 loading reaches 2.85 mmol g^{-1}, which is equivalent to one CO_2 molecule per asymmetric unit.

Interestingly, a further increase in pressure initiates a second step in the sorption isotherm with an onset pressure of approximately 37 bar. Saturation appears to be reached at 50.0 bar. A total uptake of 5.9 mmol g^{-1} at 50 bar (Figure 1) corresponds to two CO_2 molecules per host formula unit. The 35% sorption hysteresis for the second step is colossal compared to 3.2% for the first step. It is also significantly larger than the very extreme value recently reported by us (Equation S1).[17a]

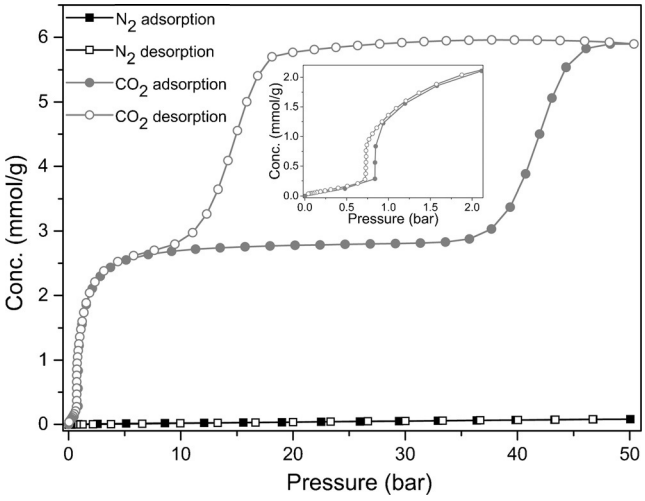

Figure 1. N_2 and CO_2 sorption isotherms for **1a** measured at 298 K.

In order to obtain structural information regarding the CO_2 sorption sites and loading-induced changes to the framework, single crystals of **1a** were pressurized with CO_2 using an environmental gas cell developed by us.[21b] In each case the single crystal within the gas cell was allowed to equilibrate at the selected pressure for one day at 298 K prior to SCXRD analysis. Although the onset of the first structural change occurs below 1 bar, a pressure of 2 bar was used in order to increase the CO_2 occupancy for improved refinement of the CO_2 guest molecules at 298 K. The diffraction patterns indicate that the crystal maintains its crystal singularity under 2 bar of CO_2 pressure (Figure S3). Similar to **1a**, the 2 bar CO_2 pressurized structure (**1b**) adopts the monoclinic space group $P2_1/c$. Comparison of the crystal structures shows lengthening of the crystallographic axes *a* (8.6890(2) Å to 9.1212(2) Å) and *c* (7.9614(2) Å to 8.1265(2) Å), with concomitant shortening of the *b* axis (19.7634(5) Å to 18.8576(4) Å) upon proceeding from **1a** to **1b**. There is also a decrease in the crystallographic β angle from 113.798(2)° to 111.963(1)° and an increase in volume from 1250.92(5) to 1296.35(5) $Å^3$ (Table S2). The asymmetric unit of **1b** remains similar to that of **1a**, except for the additional presence of a CO_2 molecule in the guest-accessible void space of **1b** (Figure 2). The CO_2 occupancy was determined to be 0.66 molecules per asymmetric unit (see the Supporting Information).

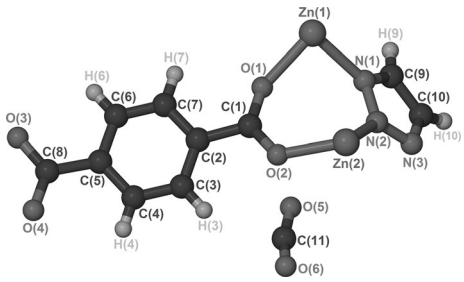

Figure 2. Perspective view of the asymmetric unit of **1b**.

Insertion of CO_2 molecules into the framework expands the pore dimensions. Most notable is the expansion of the short diagonal of the 4,4-Zn-tp rhombus-shaped network, which runs parallel to the channels occupied by CO_2: this diagonal stretches slightly from 7.95(1) Å (**1a**) to 8.12(1) Å (**1b**) (Figure 3). The trellis-like stretching mechanism[12c] elongates the channels and results in an overall increase in the amount of guest-accessible volume (Table S1).

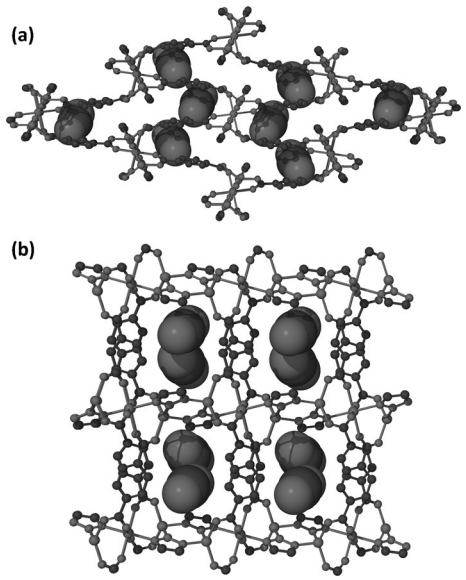

Figure 3. Perspective views of **1b** along the crystallographic *a* (a) and *c* axes (b).

Upon entering the pores of **1a**, the CO_2 molecules form strong electrostatic interactions with the framework. The closest contact occurs between the carbon atom of the guest CO_2 molecule and the oxygen atom of the carboxylate group: C11···O2 = 3.12(1) Å. In addition, there exist several other electrostatic interactions between the hydrogen atoms of the terephthalate aromatic ring and the oxygen atoms of the guest CO_2 molecules (Figure S4). In order to assess the interactions of the CO_2 guest molecules with the host framework at higher pressure, **1b** was further pressurized to 20 bar and allowed to equilibrate for 12 hours at 298 K. Although the diffraction patterns indicate that crystal singularity is maintained for **1c**, the integrity of the crystal degrades as compared to that of **1b**. At 20 bar the space group $P2_1/c$ is maintained and the site occupancy of the CO_2 molecule increases to one molecule per formula unit. The increased pressure leads to further expansion of the framework, as evidenced by expansion of all of the unit cell axes (Table S2). At 20 bar the electrostatic interaction between the oxygen atom of the carboxylate group and the carbon atom of CO_2 remains similar to that of **1b** (C11···O2 = 3.17(1) Å) (Table S3). Additionally, there exist interactions between the oxygen atoms of the CO_2 guest molecules and the hydrogen atoms of both the tp and 1,2,3-tz units (Figure S4). The crystallographic angle β decreases slightly to 111.164(4)°. Increasing the pressure to 50 bar results in loss of crystal singularity and SCXRD analysis at this pressure was therefore not possible. Pressurizing a single crystal of **1a** to only 37 bar (i.e. the onset pressure of the second step in the CO_2 sorption isotherm) also resulted in degradation of its singularity.

Pressure-gradient DSC measurements[24] at 298 K were carried out for the activated complex (**1a**) using both N_2 and CO_2 to pressures of 98 and 54 bar, respectively. In the case of N_2, no energetic event was observed, thus indicating the absence of a gate-opening structural change in **1a** (Figure S5). However, upon ramping the CO_2 pressure from 0.3 to 4 bar, a sharp exothermic peak was recorded with an onset around 0.8 bar. This exotherm is mainly due to the heat of sorption associated with the first phase-change (**1a** to **1b**/**1c**), but most likely also includes a small component associated with the structural transformation. A corresponding endothermic peak was observed upon decreasing the pressure (4 to 0.3 bar), thus implying that the first phase-change event is reversible (Figure S6). On further increasing the pressure, a second broad exothermic peak with an onset pressure of approximately 37 bar was observed. This event is associated with the second CO_2 induced phase change (**1c** to **1d**), with no further energetic events below the CO_2 saturation vapor pressure at 298 K. Upon decreasing the pressure, the onset of the corresponding endothermic peak for the desorption event associated with the transition from **1d** to **1c** occurs around 17 bar. The interval between the exothermic and endothermic events is in good agreement with the hysteresis observed in the high pressure CO_2 sorption isotherm at 298 K (Figure S7). Upon decreasing the pressure, the endothermic event is complete at approximately 7 bar, indicating reversion to the CO_2 induced phase **1c**. The pressure-gradient DSC experiments were repeated and found to be reproducible.

To substantiate the experiments described above, variable pressure PXRD patterns were recorded under CO_2 and N_2 loading at 298 K (by adapting our environmental gas cell). The bulk phase purity of activated material (**1a**) was confirmed by comparison with the simulated powder pattern generated from the single-crystal structure of the activated form (Figure S8). In the case of N_2 loading, the PXRD patterns remained unchanged to 50 bar (Figure S9). On the other hand, clear changes were observed in the PXRD patterns at various CO_2 gas pressures (Figure 4 and Figure S10). The PXRD pattern of the first CO_2 loaded sample (**1a** at 1 bar) clearly shows the occurrence of the first phase-change (**1a** to **1b**). From vacuum to 1 bar, peaks corresponding to Miller indices (100), (011) and (11−1) clearly shift towards lower 2θ values, thus indicating expansion of the framework (Figure S11). Between 1 and 20 bar the PXRD patterns remain similar. Beyond 20 bar new peaks begin to emerge in the PXRD patterns and at 40 bar the patterns change to indicate the second gas-induced phase (**1d**), which persists up to 50 bar.

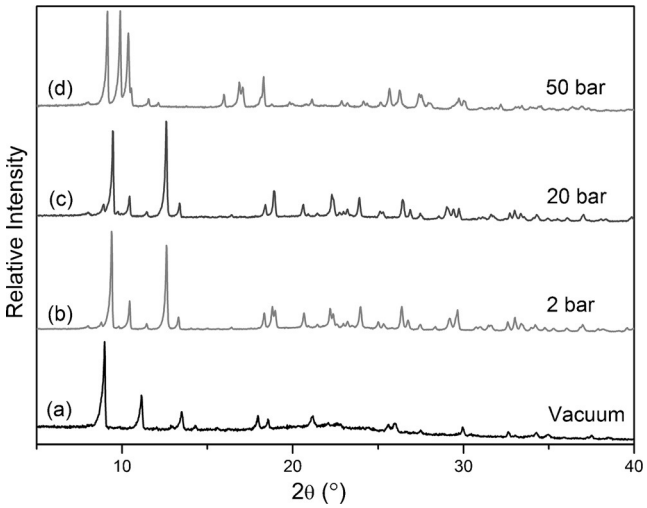

Figure 4. PXRD patterns of activated form **1a** (recorded at 298 K) under a) vacuum, b) 2 bar, c) 20 bar and d) 50 bar of CO_2.

The crystal structures for **1c** (benchmark) and **1d** were derived computationally using the activated SCXRD structure (**1a**) as initial input (Figures S12 and S13). These computationally determined structures for **1c** and **1d** were used as input structures for rigid body Rietveld refinement using the software package TOPAS 4.2 (Figures S14 and S15, Table S4).[25]

From the Rietveld refined structure **1d** it is apparent that the 4,4-Zn-tp grid continues to stretch out along the channel direction to accommodate the additional CO_2 molecules within the framework (Figure 5). The additional CO_2 molecules pack efficiently within the guest-accessible space via slipped-parallel and T-shaped guest–guest interactions (Figure 5). As expected, the framework opens up further by employing a trellis-like motion,[12c] with the acute angle of the 4,4-Zn-tp grid increasing from 38.72(1)° in **1a** to 44.20(1)° in **1c**, and then to 52.35(1)° in **1d** (Figures S16 and S17,

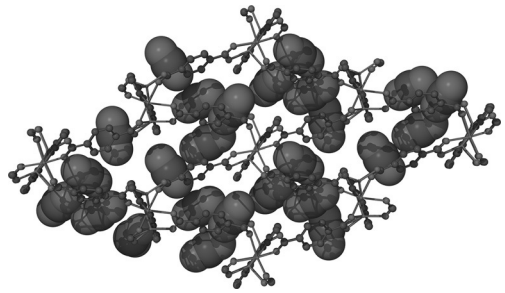

Figure 5. Perspective view of **1d** along the crystallographic *b* axis.

Table S5). The aromatic rings of the tp moieties tilt out of the channel, thus increasing the channel volume in **1d** and, consequently, the CO_2 uptake (Table S5). The increase in CO_2 uptake by **1d** is also facilitated by rotation of the 1,2,3-tz paddle moieties (Figure S16). As viewed along the *b* axis, the 1,2,3-tz paddle undergoes sufficient rotation such that two neighboring channels become interconnected (Figure S18). The space connecting the channels is occupied by two CO_2 molecules interacting with each other via slipped-parallel[17a] $CO_2 \cdots CO_2$ interactions. The transformation from **1a** to **1c** only involves a trellis-like stretching along the guest-accessible channels, whereas the transformation from **1c** to **1d** involves tilting of both the tp aromatic rings and 1,2,3-tz paddles in addition to trellis-like stretching of the 4,4-Zn-tp network.

In summary, we have shown that the breathing Zn^{II}-MOF exhibits a two-step CO_2 uptake with extreme hysteresis for the second step of the high pressure sorption isotherm recorded at 298 K. Although there are other reports on flexible frameworks that show hysteretic steps, such colossal sorption hysteresis for breathing MOFs is not very common at 298 K. We were able to obtain the CO_2 loaded structures at 2 and 20 bar (by means of in situ SCXRD studies) and 50 bar (in situ PXRD), thus providing valuable information relating to host–guest interactions in this dynamic framework. The Zn^{II}-MOF employs two structure-opening mechanisms in order to increase the CO_2 uptake: trellis-like stretching of the framework, and tilting of both the organic linkers. Understanding these mechanisms can improve our efforts to design new materials with specific pressure-induced gate-opening mechanisms in order to achieve a desired sorption property.

Acknowledgements

L.J.B. thanks the National Research Foundation (NRF) of South Africa and Stellenbosch University for financial support, as well as the Centre for High Performance Computing (CHPC) in Cape Town for the use of their resources. P.L. and H.A. acknowledge the Claude Leon Foundation and the Consolidoc Programme of the University of Stellenbosch, respectively, for financial support. CCDC 1484940, 1484941, 1484942 and 1487816, 1487817.

Keywords: CO_2 modeling · high pressure sorption · hysteresis · in situ crystallography · pressure-gradient DSC

How to cite: *Angew. Chem. Int. Ed.* **2016**, *55*, 13271 – 13275
Angew. Chem. **2016**, *128*, 13465 – 13469

[1] a) J. C. Orr, V. J. Fabry, O. Aumont, L. Bopp, S. C. Doney, R. A. Feely, A. Gnanadesikan, N. Gruber, A. Ishida, F. Joos, R. M. Key, K. Lindsay, E. Maier-Reimer, R. Matear, P. Monfray, A. Mouchet, R. G. Najjar, G.-K. Plattner, K. B. Rodgers, C. L. Sabine, J. L. Sarmiento, R. Schlitzer, R. D. Slater, I. J. Totterdell, M.-F. Weirig, Y. Yamanaka, A. Yool, *Nature* **2005**, *437*, 681 – 686; b) S. Solomon, G.-K. Plattner, R. Knutti, P. Friedlingstein, *Proc. Natl. Acad. Sci. USA* **2009**, *106*, 1704 – 1709.

[2] a) H.-C. Zhou, J. R. Long, O. M. Yaghi, *Chem. Rev.* **2012**, *112*, 673 – 674; b) A. U. Czaja, N. Trukhan, U. Müller, *Chem. Soc. Rev.* **2009**, *38*, 1284 – 1293; c) B. Li, H.-M. Wen, W. Zhou, B. Chen, *J. Phys. Chem. Lett.* **2014**, *5*, 3468 – 3479; d) R. Banerjee, A. Phan, B. Wang, C. Knobler, H. Furukawa, M. O'Keeffe, O. M. Yaghi, *Science* **2008**, *319*, 939 – 943; e) S. Sen, S. Neogi, K. Rissanen, P. K. Bharadwaj, *Chem. Commun.* **2015**, *51*, 3173 – 3176.

[3] a) G. Férey, *Chem. Mater.* **2001**, *13*, 3084 – 3098; b) M. E. Davis, *Nature* **2002**, *417*, 813 – 821.

[4] a) K. Li, D. H. Olson, J. Y. Lee, W. Bi, K. Wu, T. Yuen, Q. Xu, J. Li, *Adv. Funct. Mater.* **2008**, *18*, 2205 – 2214; b) J. Liu, P. K. Thallapally, B. P. McGrail, D. R. Brown, J. Liu, *Chem. Soc. Rev.* **2012**, *41*, 2308 – 2322.

[5] a) T. K. Maji, R. Matsuda, S. Kitagawa, *Nat. Mater.* **2007**, *6*, 142 – 148; b) R. Matsuda, R. Kitaura, S. Kitagawa, Y. Kubota, R. V. Belosludov, T. C. Kobayashi, H. Sakamoto, T. Chiba, M. Takata, Y. Kawazoe, Y. Mita, *Nature* **2005**, *436*, 238 – 241.

[6] O. K. Farha, A. Ö. Yazaydın, I. Eryazici, C. D. Malliakas, B. G. Hauser, M. G. Kanatzidis, S. T. Nguyen, R. Q. Snurr, J. T. Hupp, *Nat. Chem.* **2010**, *2*, 944 – 948.

[7] a) D.-X. Xue, A. J. Cairns, Y. Belmabkhout, L. Wojtas, Y. Liu, M. H. Alkordi, M. Eddaoudi, *J. Am. Chem. Soc.* **2013**, *135*, 7660 – 7667; b) H.-L. Jiang, Y. Tatsu, Z.-H. Lu, Q. Xu, *J. Am. Chem. Soc.* **2010**, *132*, 5586 – 5587.

[8] a) Y.-Q. Lan, H.-L. Jiang, S.-L. Li, Q. Xu, *Adv. Mater.* **2011**, *23*, 5015 – 5020; b) J. A. Mason, K. Sumida, Z. R. Herm, R. Krishna, J. R. Long, *Energy Environ. Sci.* **2011**, *4*, 3030 – 3040.

[9] a) S. B. Kayiran, F. L. Darkrim, *Surf. Interface Anal.* **2002**, *34*, 100 – 104; b) Z. Song, Y. Huang, L. Wang, S. Li, M. Yu, *Chem. Commun.* **2015**, *51*, 373 – 375.

[10] a) G. Sethia, A. Sayari, *Carbon* **2015**, *93*, 68 – 80; b) W. Xing, C. Liu, Z. Zhou, L. Zhang, J. Zhou, S. Zhuo, Z. Yan, H. Gao, G. Wang, S. Z. Qiao, *Energy Environ. Sci.* **2012**, *5*, 7323 – 7327.

[11] a) G. Férey, *Dalton Trans.* **2016**, *45*, 4073 – 4089; b) S. Horike, S. Shimomura, S. Kitagawa, *Nat. Chem.* **2009**, *1*, 695 – 704; c) Z.-Q. Jiang, G.-Y. Jiang, F. Wang, Z. Zhao, J. Zhang, *Chem. Eur. J.* **2012**, *18*, 10525 – 10529; d) M. C. Das, P. K. Bharadwaj, *J. Am. Chem. Soc.* **2009**, *131*, 10942 – 10949.

[12] a) C. Serre, F. Millange, C. Thouvenot, M. Noguès, G. Marsolier, D. Louër, G. Ferey, *J. Am. Chem. Soc.* **2002**, *124*, 13519 – 13526; b) H. Aggarwal, R. K. Das, P. M. Bhatt, L. J. Barbour, *Chem. Sci.* **2015**, *6*, 4986 – 4992; c) S. Henke, A. Schneemann, R. A. Fischer, *Adv. Funct. Mater.* **2013**, *23*, 5990 – 5996; d) A. Schneemann, V. Bon, I. Schwedler, I. Senkovska, S. Kaskel, R. A. Fischer, *Chem. Soc. Rev.* **2014**, *43*, 6062 – 6096.

[13] a) S. Yang, X. Lin, W. Lewis, M. Suyetin, E. Bichoutskaia, J. E. Parker, C. C. Tang, D. R. Allan, P. J. Rizkallah, P. Hubberstey, N. R. Champness, K. M. Thomas, A. J. Blake, M. Schröder, *Nat. Mater.* **2012**, *11*, 710 – 716; b) J.-R. Li, R. J. Kuppler, H.-C. Zhou, *Chem. Soc. Rev.* **2009**, *38*, 1477 – 1504.

[14] L. E. Kreno, K. Leong, O. K. Farha, M. Allendorf, R. P. Van Duyne, J. T. Hupp, *Chem. Rev.* **2012**, *112*, 1105 – 1125.

[15] a) B. Chen, S. Ma, E. J. Hurtado, E. B. Lobkovsky, H.-C. Zhou, *Inorg. Chem.* **2007**, *46*, 8490 – 8492; b) S. K. Ghosh, S. Bureekaew, S. Kitagawa, *Angew. Chem. Int. Ed.* **2008**, *47*, 3403 – 3406; *Angew. Chem.* **2008**, *120*, 3451 – 3454.

[16] S. Bourrelly, P. L. Llewellyn, C. Serre, F. Millange, T. Loiseau, G. Férey, *J. Am. Chem. Soc.* **2005**, *127*, 13519 – 13521.
[17] a) C. X. Bezuidenhout, V. J. Smith, P. M. Bhatt, C. Esterhuysen, L. J. Barbour, *Angew. Chem. Int. Ed.* **2015**, *54*, 2079 – 2083; *Angew. Chem.* **2015**, *127*, 2107 – 2111; b) K. L. Mulfort, O. K. Farha, C. D. Malliakas, M. G. Kanatzidis, J. T. Hupp, *Chem. Eur. J.* **2010**, *16*, 276 – 281.
[18] P. D. C. Dietzel, R. E. Johnsen, H. Fjellvåg, S. Bordiga, E. Groppo, S. Chavan, R. Blom, *Chem. Commun.* **2008**, 5125 – 5127.
[19] M.-A. Springuel-Huet, A. Nossov, Z. Adem, F. Guenneau, C. Volkringer, T. Loiseau, G. Férey, A. Gédéon, *J. Am. Chem. Soc.* **2010**, *132*, 11599 – 11607.
[20] P. L. Llewellyn, G. Maurin, T. Devic, S. Loera-Serna, N. Rosenbach, C. Serre, S. Bourrelly, P. Horcajada, Y. Filinchuk, G. Férey, *J. Am. Chem. Soc.* **2008**, *130*, 12808 – 12814.
[21] a) S. Takamizawa, Y. Takasakia, R. Miyakea, *Chem. Commun.* **2009**, 6625 – 6627; b) T. Jacobs, G. O. Lloyd, J.-A. Gertenbach, K. K. Müller-Nedebock, C. Esterhuysen, L. J. Barbour, *Angew. Chem. Int. Ed.* **2012**, *51*, 4913 – 4916; *Angew. Chem.* **2012**, *124*, 4997 – 5000; c) S. R. Miller, P. A. Wright, T. Devic, C. Serre, G. Férey, P. L. Llewellyn, R. Denoyel, L. Gaberova, Y. Filinchuk, *Langmuir* **2009**, *25*, 3618 – 3626.
[22] a) A. L. Dzubak, L.-C. Lin, J. Kim, J. A. Swisher, R. Poloni, S. N. Maximoff, B. Smit, L. Gagliardi, *Nat. Chem.* **2012**, *4*, 810 – 816; b) T. M. McDonald, J. A. Mason, X. Kong, E. D. Bloch, D. Gygi, A. Dani, V. Crocellà, F. Giordanino, S. O. Odoh, W. S. Drisdell, B. Vlaisavljevich, A. L. Dzubak, R. Poloni, S. K. Schnell, N. Planas, K. Lee, T. Pascal, L. F. Wan, D. Prendergast, J. B. Neaton, B. Smit, J. B. Kortright, L. Gagliardi, S. Bordiga, J. A. Reimer, J. R. Long, *Nature* **2015**, *519*, 303 – 308; c) R. Vaidhyanathan, S. S. Iremonger, G. K. H. Shimizu, P. G. Boyd, S. Alavi, T. K. Woo, *Science* **2010**, *330*, 650 – 653.
[23] Y. Ye, X. Wu, Z. Yao, L. Wu, Z. Cai, L. Wang, X. Ma, Q.-H. Chen, Z. Zhang, S. Xiang, *J. Mater. Chem. A* **2016**, *4*, 4062 – 4070.
[24] A. M. Plonka, D. Banerjee, W. R. Woerner, Z. Zhang, N. Nijem, Y. J. Chabal, J. Li, J. B. Parise, *Angew. Chem. Int. Ed.* **2013**, *52*, 1692 – 1695; *Angew. Chem.* **2013**, *125*, 1736 – 1739.
[25] Bruker, AXS, Karlsruhe, TOPAS V4.2, General profile and structure analysis software for powder diffraction data, User's Manual, **2009**.

Received: July 21, 2016
Published online: September 16, 2016

